ACS Sustainable Chemistry & Engineering

Research Article

pubs.acs.org/journal/ascecg

Comparative Investigation on Photoreactivity and Mechanism of Biogenic and Chemosythetic Ag/C_3N_4 Composites under Visible Light Irradiation

Ke Tian, Wu-Jun Liu, and Hong Jiang*

CAS Key Laboratory of Urban Pollutant Conversion, Department of Chemistry, University of Science and Technology of China, No.96, Jinzhai Road, Hefei 230026, China

Supporting Information

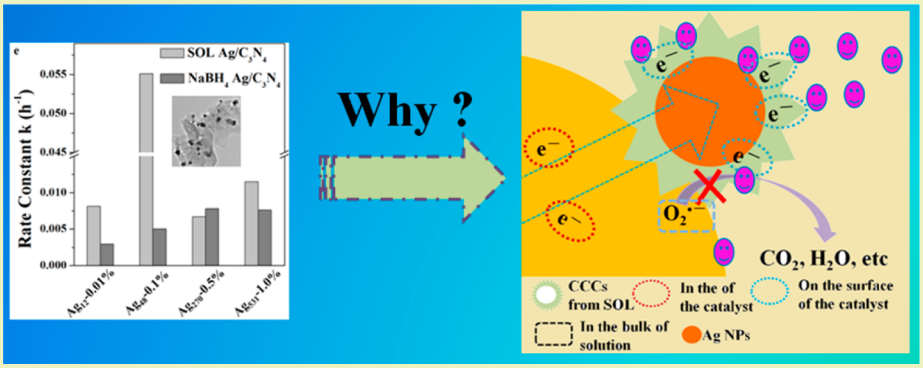

ABSTRACT: A Ag/C_3N_4 nanocomposite with optimum Ag content is an efficient and green photocatalyst for pollutant degradation under visible light irradiation. In this study, we synthesized Ag NPs using $NaBH_4$ and the squeezed out liquid (SOL) of plant biomass. The Ag NPs thus obtained have been loaded to C_3N_4 to form Ag/C_3N_4 nanocomposites that show superior photocatalytic performance toward Rhodamine B (RhB) under visible light irradiation. The photocatalytic activity of both biogenic and chemogenic Ag/C_3N_4 nanocomposites with different Ag contents is compared. Results show that the biogenically synthesized Ag/C_3N_4 exhibits better photocatalytic performance than the chemosynthetic composite. Of all the different nanocomposites prepared in this study, Ag_{48}/C_3N_4 (0.048% of Ag content) exhibits excellent photoreactivity, with a reaction rate constant (k) 7-fold higher that the chemosynthetic Ag/C_3N_4. The observed improvement in the photoreactivity is mainly attributed to the high dispersion of Ag NPs on C_3N_4, facilitated by the organic compounds in SOLs. Besides, these organic compounds also enhance the photoreactivity of the catalyst by providing adsorption sited for RhB molecules and by shifting the Fermi level to more negative potential.

KEYWORDS: *Graphitic carbon nitride, Photoreactivity, Nanocomposite, Pollutants, Ag NPs*

INTRODUCTION

The engineered Ag NPs were widely used in different industries, such as catalysis and disfection.[1−3] Ag NPs are generally synthesized through the chemical reduction process, during which the expensive, toxic, or flammable reducing agents, such as $NaBH_4$, NH_2-NH_2, and H_2, are often used.[4,5] Thus, some researchers focused on the synthesis of different noble metallic NPs using plant extracts because they usually contain reductive enzymes, amino acids, vitamins, polysaccharides, and organic acids. Besides, they can also act as capping agents during the synthesis process of NPs.[5−7]

On the other hand, graphitic carbon nitride (C_3N_4) is an green photocatalyst for water splitting and pollutant degradation because it is metal-free and highly stable in both acid and alkaline environments by the formation of the conjugated graphitic planes by the sp^2 hybridization of C and N atoms.[8−14] Nevertheless, because of the quick recombination of photogenerated charge carriers, the photocatalytic activity of the C_3N_4 is still low.

Lately, Ag NPs-loaded graphitic carbon nitride (C_3N_4) is reported to be a green and stable photocatalyst for the degradation of pollutants.[15,16] The addition of Ag NPs is expected to improve the photocatalytic performance of C_3N_4 by facilitating the charge separation process.[14,17] In principle, the addition of Ag NPs to C_3N_4 can shift the equilibration between the Fermi levels of the metal and the conduction band of C_3N_4 to a more negative potential, making electron transfer to an acceptor (e.g., O_2 and H_2O_2) energetically more favorable and thus increasing the efficiency of charge separation and transfer.[18,19] Furthermore, the difference in Fermi levels of the

Received: October 10, 2014
Revised: December 10, 2014
Published: December 24, 2014

DOI: 10.1021/sc500646a
ACS Sustainable Chem. Eng. 2015, 3, 269−276

metal and C_3N_4 favors the formation of a Schottky barrier, which can act as an electron trap to decrease the electron−hole recombination following a photoexcitation.

In such a system, the photoreactivity of Ag/C_3N_4 is often influenced by the loading concentration of Ag NPs in Ag/C_3N_4. Given the consideration that Ag is a noble metal and that its leakage might lead to environmental risk,[20,21] it is highly imperative to reduce the amount of Ag additive, yet maintain the photoreactivity of the material. Ge et al. reported the optimum chemogenic Ag doping amount on C_3N_4.[15,16] Given the advantages of biogenic synthetic Ag/C_3N_4, we believe that it is possible to further reduce the Ag additive, yet realize improved photoreactivity in Ag/C_3N_4. However, there is no systematic comparison on photoreactivity between chemogenic and biogenic synthetic Ag/C_3N_4, and the study of optimization of Ag additive in biogenically synthesized Ag/C_3N_4 is still unavailable.

Therefore, the main objective of the present work is to experimentally compare the photoreactivity of chemogenic and biogenic synthesized Ag/C_3N_4 photocatalysts. To this end, we (1) synthesized Ag/C_3N_4 photocatalysts using $NaBH_4$ and the squeezed out liquid (SOL) of watermelon rind, (2) compared their photoreactivity toward a model pollutant Rhodamine B (RhB) under visible light irradiation, (3) evaluated the optimum biogenic Ag doping amount on C_3N_4, and (4) explored the role of SOL in enhancing the photoreactivity of biogenically synthesized Ag/C_3N_4.

EXPERIMENTAL SECTION

Materials. All chemicals and reagents used in this work were of analytical grade and purchased from Sinopharm Chemical Reagent Co., Ltd., China. $AgNO_3$ was used as a precursor for the synthesis of Ag NPs. Three typical biomass wastes, namely, alligator weed, watermelon rind, and Chinese cabbage, were squeezed with a juicer to obtain the SOLs. Dicyandiamide was used as a precursor for the synthesis of the graphitic carbon nitride (g-C_3N_4). In a typical process, 5.0 g of dicyandiamide powder was placed in a ceramic crucible and heated to a temperature of 823 K within 30 min. The precursor was maintained at this temperature for 3 h in a muffle. Subsequently, they were cooled to room temperature to obtain the final product g-C_3N_4.[14]

Synthesis of Ag/C_3N_4. Ag NPs were synthesized by mixing an equal volumetric (10 mL) amount of 0.01 M silver nitrate and the SOLs under continuous stirring for 24 h. Thereafter, the resulting mixture was directly used for the synthesis of the Ag/C_3N_4 without further separation and purification. The general procedure for the synthesis of Ag/C_3N_4 is as follows: A mixture containing 0.5 g of g-C_3N_4 dispersed in 20 mL of deionized water was added to a 100 mL conical flask as the substrate. Following that, a predetermined quantity of the SOL−Ag NPs mixture (mass ratios of Ag NPs to g-C_3N_4 are 0.01%, 0.1%, 0.5%, and 1%) was added to the g-C_3N_4 dispersion under continuous stirring for 20 h. The resulting mixture was filtered to separate out the solid, which was then washed three times with ethanol and water successively. Finally, the solid was dried overnight in an oven at 343 K.

Characterization. The Ag content in the Ag/C_3N_4 nanocomposite was analyzed by inductively coupled plasma-sector field mass spectrometry (ICP-SFMS, Plasma Quad 3, Thermo-VG Elemental, U.K.). The crystallinity and phase of Ag/C_3N_4 was analyzed by X-ray diffraction (XRD, MXPAHF, Rigaku, Japan) using a nickel-filtered Cu Kα radiation source (30 kV/160 mA, λ = 1.54056 Å). The samples were scanned in the 2θ range of 10° to 70°, at a scan rate of 0.02/s. The chemical state of the Ag/C_3N_4 nanocomposite was analyzed by X-ray photoelectron spectroscopy (XPS, ESCALAB250, Thermo-VG Scientific, U.K.) using monochromatized Al Kα radiation (1486.92 eV). The surface morphology and chemical composition of the Ag/C_3N_4 nanocomposite was analyzed by field emission transmission electron microscopy (FETEM, JEM-2100F, JEOL, Japan) coupled with energy dispersive X-ray (EDX) spectrometry. Ultraviolet−visible (UV−vis) diffuse reflection spectra (DRS) were recorded using a deep ultraviolet−visible−near-infrared spectrophotometer (DUV-3700, SHIMADZU, Japan) in the wavelength range of 200−800 nm. $BaSO_4$ was used as the standard. The photoluminescence (PL) spectra of the samples were obtained by a steady state spectrofluorometer (FLUOROLOG-3-TAU, Jobin Yvon, France) at an excitation wavelength of 450 nm.

Photocatalytic Activity Evaluation. The photocatalytic activity of the prepared Ag/C_3N_4 nanocomposite was evaluated toward RhB under visible light irradiation (light source: Xe lamp, XD300, Nanjing yanam special lighting electrical appliance factory). In a typical experiment, 50 mg of the catalyst was mixed with 100 mL of RhB solution at different concentrations (2.5−50 mg L^{-1}).[22] Before irradiation, the suspensions were stirred for 30 min in the dark to establish absorption−desorption equilibrium between RhB and the catalyst surface. All the experiments were performed under constant stirring at room temperature. During photocatalytic reaction, 5 mL aliquots of the solution was sampled every 30 min and analyzed using a UV−vis spectrophotometer (UV-1700, Phenix Optical Scientific Instrument Co., Ltd. China). The characteristic absorption peak of RhB was observed at 553.5 nm.[23] After completion of the photodegradation process, the catalyst was separated from the reaction mixture by centrifugation. The separated catalyst was washed thrice with deionized water and dried overnight in an oven at 378 K for use in the next cycle.

RESULTS AND DISCUSSION

Characterizations. The morphology of the biogenic Ag NPs, as observed by using TEM, indicates a relatively uniform size and shape, with the particle diameter ranging from 15−35 nm (Figure 1a and inset). The TEM photographs of Ag NPs

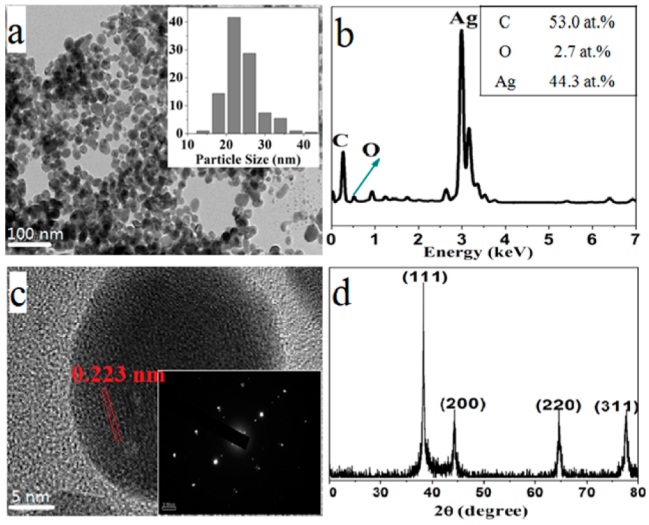

Figure 1. (a) Low-resolution TEM images of Ag NPs (inset: particle size distribution),.(b) EDX pattern of the Ag NPs (inset: atomic percentage of different element). (c) High-resolution TEM images of the Ag NP (inset: electron-diffraction pattern). (d) XRD pattern of the Ag NPs.

systhesized by using *Alternanthera philoxeroides*, Chinese cabbage, and the mixture of SOLs show no obvious difference on distribution and morphology, suggesting that biomass types have a negligible effect on the synthesis of Ag NPs (Figures S1 and S2, Supporting Information). The composition of the Ag NPs is analyzed by using EDX (Figure 1b), which indicates the presence of a considerable amount of carbon and oxygen in

DOI: 10.1021/sc500646a
ACS Sustainable Chem. Eng. 2015, 3, 269−276

addition to Ag. The carbon and oxygen in the sample can be attributed to the organic compounds capping the surface of the Ag NPs. Figure 1c shows the lattice image of the prepared Ag NPs, which indicates a *d* spacing of 0.223 nm, corresponding to the typical (111) crystal phase of Ag.[15] The XRD pattern of the Ag NPs shown in Figure 1d exhibits four characteristic peaks at 2θ of 38°, 44°, 65°, and 77°, which can be attributed to the (111), (200), (220), and (311) lattice plane of metallic Ag, respectively.

The C:N atomic ratio in the prepared C_3N_4 is 0.72 (Table S1, Supporting Information), which is close to the theoretical ration of C_3N_4. The TEM image of raw g-C_3N_4 shown in Figure 2a indicates a layered structure formed by stacking up of

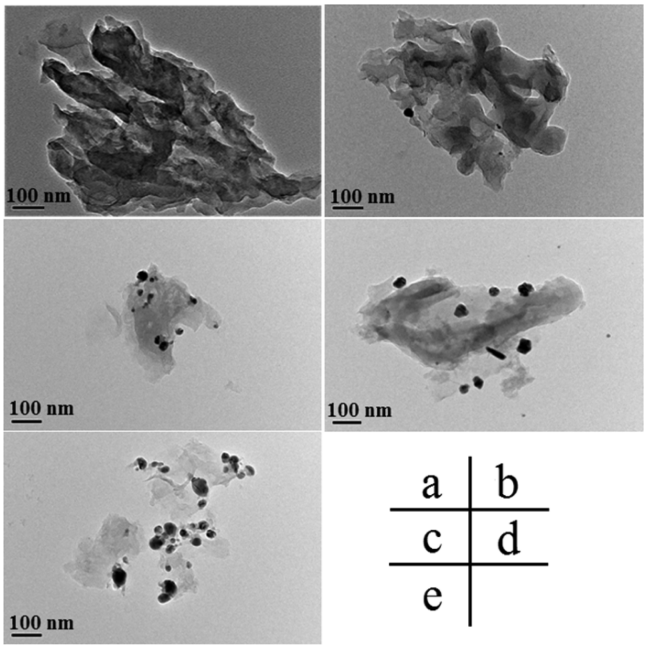

Figure 2. Low-resolution TEM images of (a) C_3N_4, (b)Ag_{12}/C_3N_4, (c) Ag_{48}/C_3N_4, (d) Ag_{270}/C_3N_4, and (e) Ag_{531}/C_3N_4.

the graphitic-like planes. With Ag loading, the TEM image of the Ag/C_3N_4 nanocomposite (Figure 2b and 2c) shows some dark particles, indicating that the Ag NPs are overlaid on the surface or the interlayers of g-C_3N_4 to form Ag/C_3N_4. Ag_{12}/C_3N_4, Ag_{48}/C_3N_4, Ag_{270}/C_3N_4, and Ag_{531}/C_3N_4 denote that the content of the silver NPs on C3N4 surface is 0.012%, 0.048%, 2.70%, and 5.31%, respectively, according to the XPS (Table S1, Supporting Information). With increase in Ag content, the Ag NPs in Ag/C_3N_4 tend to aggregate together (Figure 2d and 2e). For Ag content corresponding to 0.01%, almost all the Ag NPs in suspension are loaded on the surface or the interlayer of g-C_3N_4, while only 50% of Ag NPs are loaded for other concentrations of Ag NPs. This phenomenon may be related to the nature of C_3N_4 in the adsorption of Ag NPs. For the Ag content of 0.01%, the dosage of C_3N_4 can provide enough adsorptive sites for Ag, and all the Ag NPs in the suspension can be adsorbed by C_3N_4. While with an increase in Ag contents, the C_3N_4 used in the adsorption process cannot offer enough adsorption sites for all the Ag, and the deposition of Ag on C_3N_4 decreased with an increase in Ag concentrations.

XRD patterns of the Ag/C_3N_4 nanocomposites with different concentrations of Ag NPs are shown in Figure S3 of the Supporting Information. The diffraction peak at 2θ of 13° ((100) diffraction plane) and 28° ((002) diffraction plane) are the characteristic peaks of g-C_3N_4, which can be attributed to the in-plane structural packing motif of tri-s-triazine units and the interlayer stacking of the conjugated aromatic system, respectively.[24] The characteristic peaks at 38° and 46° correspond to the (111) and (200) planes of metallic Ag, respectively. At very low concentrations of Ag, the XRD pattern does not show peaks corresponding to Ag in the nanocomposite. This can be attributed to the fact that the XRD signals may be covered by the supports at very low metal contents. Similar results have been reported in other relevant work.[16]

The surface composition and chemical state of the Ag/C_3N_4 nanocomposites are further investigated by XPS. The XPS Ag 3d spectrum shown in Figure 3 (peak fitting in the regions of 364−378 eV) has two peaks at 367 and 374 eV, corresponding to metallic Ag.[25] The peak at 368 eV can be attributed to Ag(I), suggesting some formation of Ag_2O on the surface of metallic

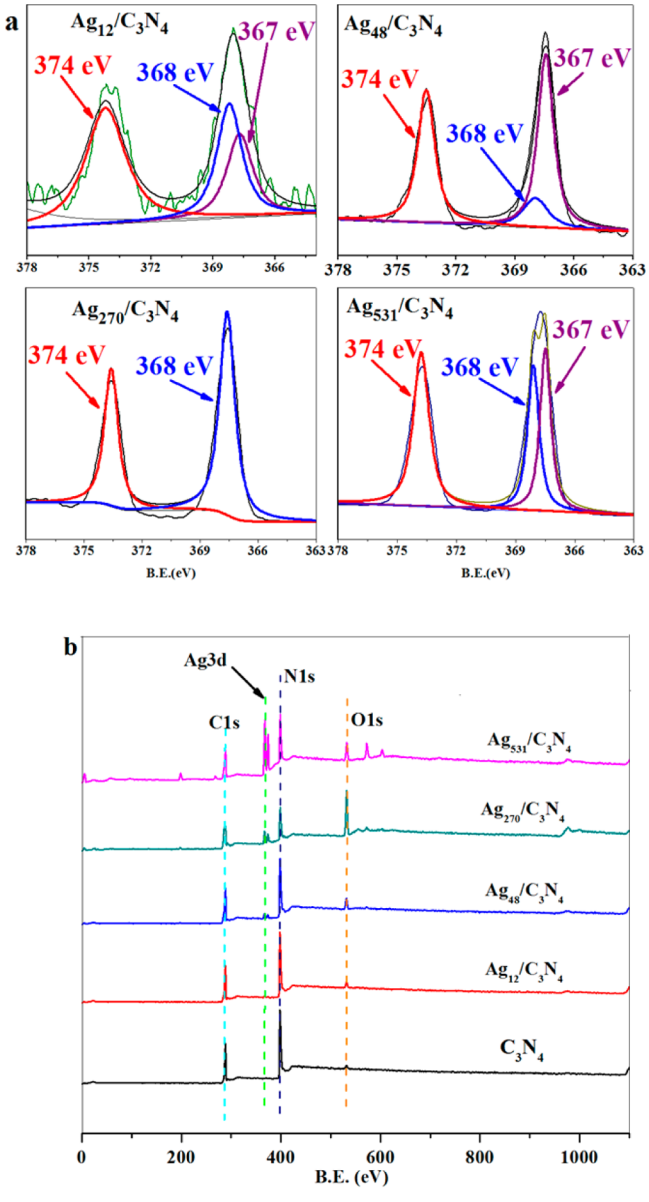

Figure 3. (a) XPS Ag 3d of spectra. (b) XPS survey spectra of the Ag/C_3N_4 nanocomposites.

DOI: 10.1021/sc500646a
ACS Sustainable Chem. Eng. 2015, 3, 269−276

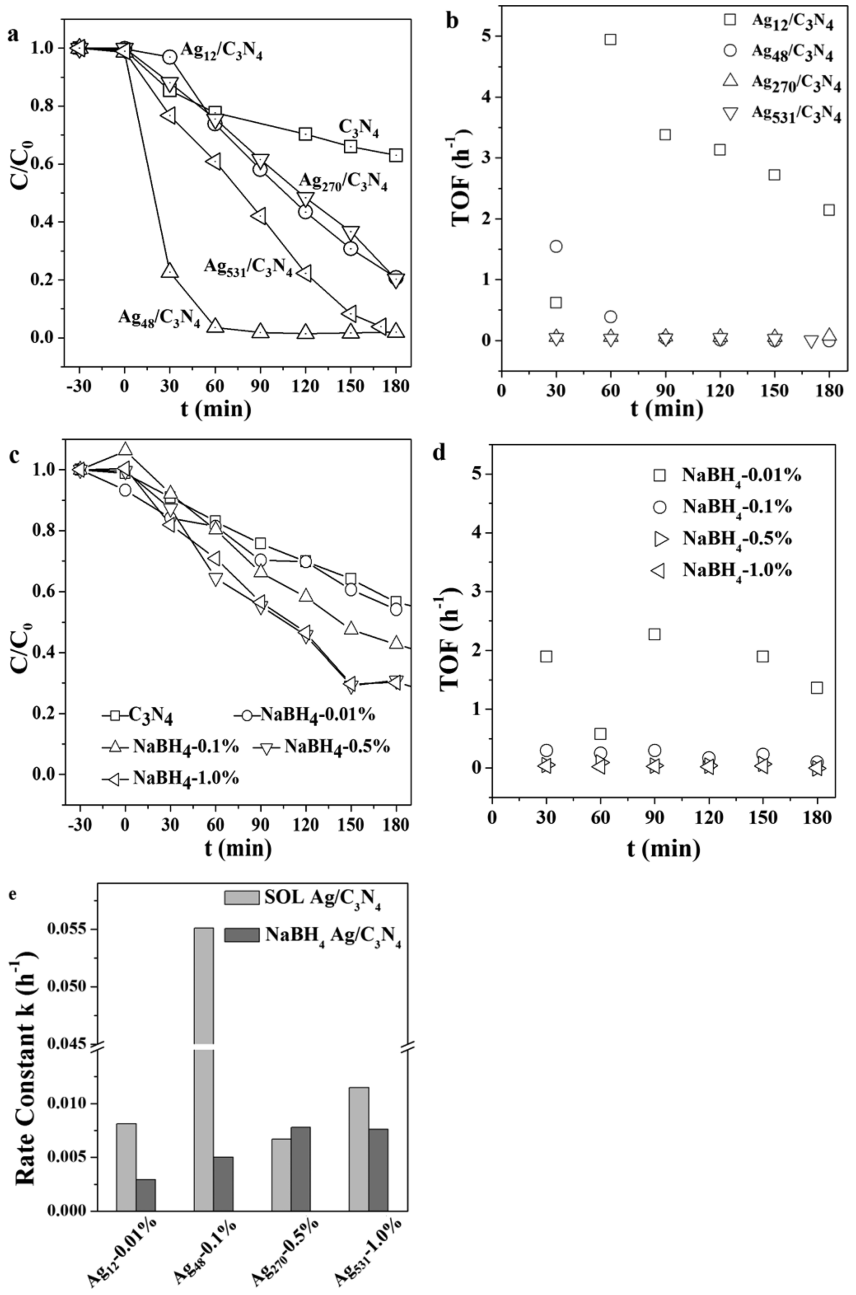

Figure 4. (a) Photocatalytic activity of biogenically synthesized Ag/C_3N_4. (b) TOF of biogenically synthesized Ag/C_3N_4. (c) Photocatalysis activity of Ag/C_3N_4 obtained by chemosynthesis. (d) TOF of chemosynthetic Ag/C_3N_4. (e) Reaction rate constants (k) of biogenic and chemosynthetic Ag/C_3N_4. (Photodegradation experiment conditions: 0.5 g L^{-1} catalyst, 2.5 mg L^{-1} RhB, 30 min in the dark, and 180 min irradiation with visible light).

Ag (Figure S4, Supporting Information). Figure 3b shows the XPS survey spectrum of the Ag/C_3N_4 nanocomposites. As shown, the C/N ratio increases with an increase in Ag concentration. This can be ascribed to the presence of organic compounds, such as soluble enzymes, amino acids, vitamins, polysaccharides, and organic acids, on the surface of biogenic Ag NPs.

Photocatalytic Activity. The photocatalytic activity of the biogenic Ag/C_3N_4 nanocomposites with different concentrations of Ag was evaluated toward RhB under visible light irradiation. The adsorption of RhB in a dark environment is negligible (Figure S5, Supporting Information). Of all the samples prepared in this study, namely, Ag_{12}/C_3N_4, Ag_{48}/C_3N_4, Ag_{270}/C_3N_4, and Ag_{531}/C_3N_4, the nanocomposite with 0.48% Ag content, (Ag_{48}/C_3N_4) shows better activity. The Ag_{48}/C_3N_4 nanocomposite completely degraded RhB within 60 min, while under the same conditions, the Ag_{12}/C_3N_4, Ag_{270}/C_3N_4, and Ag_{531}/C_3N_4 nanocomposites degraded only 24%, 26%, and 39% of RhB, respectively. The degradation rate of these nanocomposites reached 80% with reaction time increaseed to 180 min. On the other hand, raw C_3N_4 degraded only 30% of RhB in 180 min under the same experimental conditions. This clearly indicates that the introduction of Ag to the C_3N_4 significantly increases its photoreactivity. Among all the Ag/C_3N_4 nanocomposites prepared in this study, the Ag_{48}/C_3N_4 nanocomposite exhibited the highest reaction rate constant (k) and turnover frequency (TOF) (Figure 4b and e; Table S2, Supporting Information). This implies that the Ag content of

DOI: 10.1021/sc500646a
ACS Sustainable Chem. Eng. 2015, 3, 269−276

0.48% is the optimum concentration for better photocatalytic activity. The observed enhancement in the photocatalytic activity of Ag_{48}/C_3N_4 can be attributed to the optimum Ag concentration and favorable dispersion of Ag NPs on the surface of C_3N_4. As shown from the TEM images in Figure 2, the Ag NPs in Ag_{12}/C_3N_4 and Ag_{48}/C_3N_4 are almost monodispersed, while the Ag NPs in Ag_{270}/C_3N_4 and Ag_{531}/C_3N_4 are rather agglomerated or stacked up. The uniform dispersion of Ag NPs is expected to promote optical conversion efficiency, whereas the agglomeration of Ag NPs would shade each other, thus reducing optical conversion efficiency. Although it is evident that Ag_{12}/C_3N_4 has the maximum degradation rate with unit molar Ag, this photocatalyst is not the most effective one due to the very low concentration of Ag.

For comparison, we analyzed the RhB photodegradation efficiency of chemosynthetic Ag/C_3N_4 nanocomposites synthesized by $NaBH_4$ reduction. Results indicate that both the efficiency and photodegradation rate of the chemosynthetic Ag/C_3N_4 nanocomposite is lower than those of biogenically synthesized Ag/C_3N_4 (Figure 4c and d). The maximum k value of chemosynthetic Ag/C_3N_4 is 7.8×10^{-3} min^{-1}, which is much lower than that of biogenic photocatalyst ($k = 55.1 \times 10^{-3}$ min^{-1}) (Figure 4e). The observed improvement in the photoreactivity of biogenically synthesized composite could be mainly attributed to the effect of organic molecules in the biogenic Ag/C_3N_4. The soluble enzymes, amino acids, vitamins, polysaccharides, and organic acids in the SOL not only act as reducing agents but also serve as dispersing and capping agents, significantly improving the dispersion of Ag NPs on the C_3N_4 surface.[26] The obvious aggregation of chemogenic Ag NPs on C_3N_4 is observed by TEM images, which verified the aforementioned hypothesis (Figure S6, Supporting Information). On the other hand, as reported in much literature, the size of the nanoparticles has great effects on their catalytic activity;[27−29] small particle size may be in favor of catalytic activity because more active catalytic sites can be offered in the nanoparticles of small size. Comparing the particle size distribution of chemogenic and biogenic catalysts (Figure S7, Supporting Information; Figure 2a), the average size of chemogenic Ag NPs is much higher than that of biogenic ones. This may be another factor contributing to the higher catalytic activity of biogenic Ag/C_3N_4.

One of the main disadvantages in photodegradation is that most of the photocatalysts are only efficient in low concentrations of wastewater. Therefore, in this study, we analyzed the photodegradation activity of the prepared composites in different concentrations of RhB (Figure S5, Supporting Information). As predicted, the rate constant decreases with an increase in RhB concentration 5. Nevertheless, the degradation efficiency of the nanocomposite is still better toward a high concentration of RhB. More quantitatively, approximately 60% of RhB was degraded in 3 h with 20 mg L^{-1} of nanocomposite in solution. This clearly indicates that biogenically synthesized Ag/C_3N_4 could potentially be used in the treatment of wastewater.

Recycling Test. One of the most important requirements of a heterogeneous catalyst is its feasibility to be separated and reused easily. In this work, we evaluated the reusability and repeated performance of the Ag/C_3N_4 nanocomposite (Figure 6). Results indicate that the Ag/C_3N_4 nanocomposite exhibits the same degradation performance toward RhB (complete degradation within 60 min) even after recycling the sample five times. This clearly indicates the stability of the Ag/C_3N_4 nanocomposite for the photocatalytic degradation process. In addition, the chemical states of Ag in the biogenic Ag/C_3N_4 surface is another important index denoting the stability of Ag/C_3N_4. Generally speaking, the photocatalysts containing Ag are unstable under light irradiation. After a photocatalytic reaction, Ag nanoparticles are formed due to Ag+ reacting with e^-. We compared the chemical states of Ag in the biogenic Ag/C_3N_4 surface before and after recycling by XPS (Figure S8, Supporting Information). The peak of the Ag(I) species (B.E. 368.6 eV) of recycled Ag/C_3N_4 is stronger than that of the original one, indicating that the Ag in the Ag/C_3N_4 catalyst is oxidized to some extent. In Figure 6, it is shown that the existence of Ag(I) has little impact on the stability of the as-prepared catalyst.

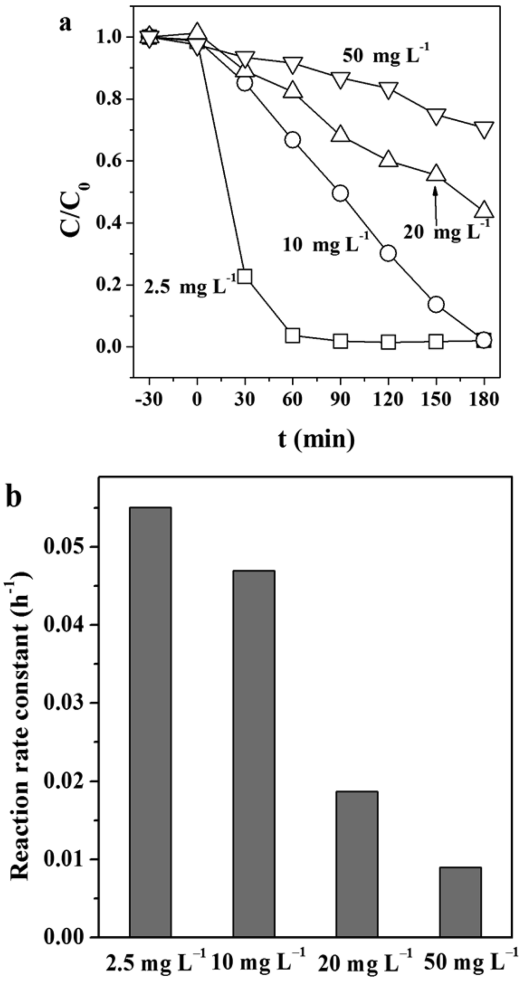

Figure 5. Effect of RhB concentration. (Photodegradation experiment conditions: 0.5 g L^{-1} catalyst, 30 min in the dark, and 180 min irradiation with visible light).

Photocatalytic Mechanism. *Effect of Organic Compounds.* As mentioned earlier, the XPS (Figure 3b) and EDX (Figure 1b) spectra of the biogenically synthesized Ag/C_3N_4 nanocomposite indicate the presence of organic compounds, making it different from the chemosynthetic composites. This could be the main reason for the observed improvement in photocatalytic activity of the biogenically synthesized Ag/C_3N_4. It is believed that the organic molecules on the surface of the nanocomposite tend to attract the target RhB molecules in solution via hydrogen bonding or complexation.[30] Besides, the existence of organic compounds on the surface of the catalyst

DOI: 10.1021/sc500646a
ACS Sustainable Chem. Eng. 2015, 3, 269−276

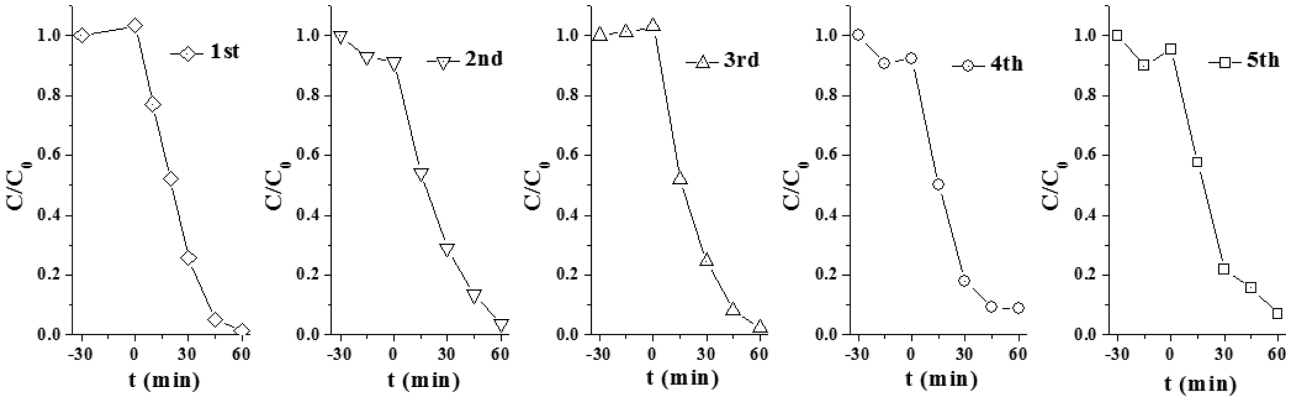

Figure 6. Reusability of Ag_{48}/C_3N_4. (Photodegradation experiment conditions: 0.5 g L^{-1} catalyst, 2.5 mg L^{-1} RhB, 30 min in the dark, and 180 min irradiation with visible light).

could shift the Fermi level to more negative potential,[31,32] favoring the transfer of photoexcited electrons to the Ag NPs. Furthermore, the organic compounds hinder the recombination of the photoexcited electron−hole pair, thereby enhancing the reducing ability of Ag/C_3N_4. To examine the effect of organic matter on the photoreactivity of C_3N_4, photodegradation experiments on C_3N_4 with and without organic matter were conducted (Figure S9, Supporting Information). It is shown that there is no significant difference between the photocatalytic activity of C_3N_4 and biogenic C_3N_4, suggesting that the reducing sugars in the SOL cannot enhance the photocatalytic activity of the pure C_3N_4.

Effect of Radicals. Under visible light irradiation, the photoinduced charges from the C_3N_4 semiconductor are transferred to the superficial Ag NPs, wherein they dissociate the water molecules to form radicals (e.g., $^{\bullet}OH$ and $O_2^{\bullet-}$).[15,33,34] To investigate the impact of radicals on the photocatalytic degradation of RhB, we used different radical scavengers (HCO_3^-, methanol, t-butanol, and p-benzoquinone) during the photodegradation of RhB.[34] As shown in Figure 7, the degradation of RhB was almost suppressed by p-benzoquinone, a scavenger of $O_2^{\bullet-}$. This indicates that $O_2^{\bullet-}$ in the aqueous solution is an important factor in the degradation of RhB. Besides, the degradation of RhB was remarkably suppressed by the HCO_3^- that react with positive hole (h^+) and combine with the $^{\bullet}OH$ on the surface of catalyst. This suggests that h^+ or surface-adsorbed $^{\bullet}OH$ play an important role in the reaction. Meanwhile, we determined $^{\bullet}OH$ in the solution using coumarin as a trapping agent and found that with the catalysis of biogenic Ag/C_3N_4, the $^{\bullet}OH$ radicals can form within 10 min, and the contents were kept almost unchanged for 30 min (Figure S10, Supporting Information). Figure 7 shows that both of methanol and t-butanol, which can scavenge $^{\bullet}OH$ in solution and hardly adsorbed on the catalyst, have no obvious effect on the degradation of RhB, indicating that $^{\bullet}OH$ in bulk solution has very little influence on the photodegradation of RhB.

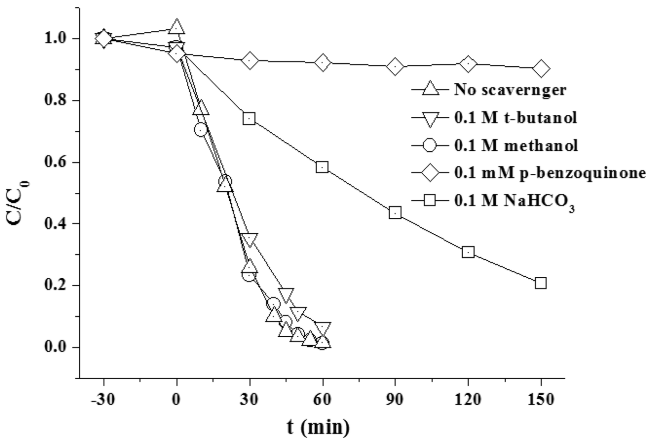

Figure 7. Effect of different scavengers on degradation of RhB by Ag_{48}/C_3N_4. (Photodegradation experiment conditions: 0.5 g L^{-1} catalyst, 2.5 mg L^{-1} RhB, 30 min in the dark, and 150 min irradiation with visible light).

Effect of Oxygen Vacancy. The PL spectra of C_3N_4 show a peak at 450 nm, which could be attributed to the trapping state emission of oxygen vacancy in the C_3N_4 crystal.[11] The photoexcited charge-carrier trapping and recombination, as analyzed using PL emission spectroscopy (Figure S11, Supporting Information), indicates that the peak of C_3N_4 is the maximum. The PL signal intensities of the catalysts decreased with a decrease in Ag content, indicating a decrease in oxygen vacancies. It is reported that the defect-related PL emission in the semiconductor can be weakened by the surface-loaded metallic NPs due to a charge transfer effect from the semiconductor to metallic NPs.[34−36] The weakening of PL emission intensity in Ag/C_3N_4 is caused by the effective charge-carrier transfer from the Ag NPs to the C_3N_4 crystal, which in turn is expected to improve the photocatalytic activity of Ag/C_3N_4.

Effect of Band Gap. The photocatalytic performance of the nanocomposite can be influenced by the absorbance, redox potential, and mobility of charge carriers,[26,37] which are determined by its electronic band structure. Therefore, the electronic band structure of Ag/C_3N_4 was determined from the UV−vis diffuse reflection spectrum and the valence band spectrum of different Ag/C_3N_4 (Figures S12 and S13, Supporting Information).[26] As evidenced from Figure S13 of the Supporting Information, the electronic band gap narrows gradually with an increase in Ag content, consistent with the previous reports.[15,21] In principle, the valence band edge is favorably associated with the oxidation ability of h^+ on the surface of catalyst. Hence, the introduction of Ag should improve the oxidation ability of Ag/C_3N_4, or in other terms, the oxidation ability of the catalyst should be elevated with an increase in Ag content. On the contrary, the experimental observations (Figure 4) do not support this hypothesis. This abnormal phenomenon can be attributed to the following two

DOI: 10.1021/sc500646a
ACS Sustainable Chem. Eng. 2015, 3, 269−276

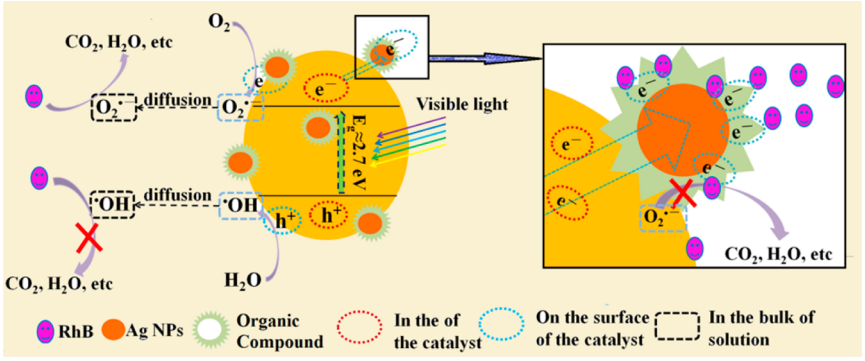

Figure 8. Mechanism underlying the degradation of RhB by Ag/C_3N_4 photocatalyst in solution.

factors: The first explanation is based on the dispersion of Ag NPs on C_3N_4. Higher Ag content in the composite may result in aggregation of the Ag NPs, thereby reducing the activity of the catalyst. Another explanation is that h^+ does not play an important role in the degradation of RhB.

On the basis of the aforementioned experiments and measurements, we have proposed the mechanism underlying this phenomenon (Figure 8). Upon visible light irradiation, the photoexcited electrons in C_3N_4 are transferred to Ag NPs, which react with water to produce $O_2^{\bullet-}$. The $O_2^{\bullet-}$ ions diffuse into the bulk solution and react with the RhB molecules. Some RhB molecules, which are adsorbed on the surface of Ag/C_3N_4 via the organic compounds, are degraded by h^+ or the surface-adsorbed •OH. Several factors influence the photoreactivity of biogenically synthesized Ag/C_3N_4, among which the dispersion of Ag NPs is a dominant factor. Commonly, the mineralization degree of organic pollutants by photocatalytic degradation is relatively low. In this study, approximate 60% of RhB can be mineralized after 180 min by biogenic Ag/C_3N_4 (Figure S14, Supporting Information).

CONCLUSIONS

In summary, the photocatalytic activity of the Ag/C_3N_4 nanocomposites with different concentrations of Ag is investigated toward RhB solution. Results show that the biogenically synthesized Ag/C_3N_4 nanocomposites exhibit better photocatalytic activity than the nanocomposite prepared by chemosynthesis. Of all the different nanocomposites prepared in this study, the Ag/C_3N_4 composite containing 0.48% Ag exhibits excellent photoreactivity under visible light irradiation. The observed improvement in the photoreactivity is mainly attributed to the high dispersion of Ag NPs on the surface of C_3N_4 due to the effect of organic compounds in SOLs. The RhB molecules are mainly photocatalyzed by the $O_2^{\bullet-}$ in bulk solution and •OH on the surface of Ag/C_3N_4. Besides, polyphenols, ascorbic acid, and various reducing sugars in the SOL also enhanced the photoreactivity of the catalyst.

ASSOCIATED CONTENT

Supporting Information

Detailed properties of biogenic and chemogenic Ag/C_3N_4, degradation results of RhB by C_3N_4 and C_3N_4–SOL, photoluminescence emission spectra, UV–vis diffuse reflection spectrum, and electronic band structure of different Ag/C_3N_4. This material is available free of charge via the Internet at http://pubs.acs.org.

AUTHOR INFORMATION

Corresponding Author

*E-mail: jhong@ustc.edu.cn. Fax: 86-551-63607482.

Notes

The authors declare no competing financial interest.

ACKNOWLEDGMENTS

The authors gratefully acknowledge financial support from the National 863 Program (2012AA063608-01), National Key Technology R&D Program of the Ministry of Science and Technology (2012BAJ08B00), and Key Special Program on the S&T for the Pollution Control and Treatment of Water Bodies (2012ZX07103-001).

REFERENCES

(1) Xiong, Z.; Ma, J.; Ng, W. J.; Waite, T. D.; Zhao, X. S. Silver-modified mesoporous TiO_2 photocatalyst for water purification. *Water Res.* **2011**, *45*, 2095–2103.

(2) Kulkarni, A. A.; Bhanage, B. M. Ag@AgCl nanomaterial synthesis using sugar cane juice and its application in degradation of Azo Dyes. *ACS Sustainable Chem. Eng.* **2014**, *2*, 1007–1013.

(3) Ma, N.; Zhang, Y.; Quan, X.; Fan, X.; Zhao, H. Performing a microfiltration integrated with photocatalysis using an Ag-TiO_2/HAP/Al_2O_3 composite membrane for water treatment: Evaluating effectiveness for humic acid removal and anti-fouling properties. *Water Res.* **2010**, *44*, 6104–6114.

(4) Kvítek, L.; Prucek, R.; Panáček, A.; Novotný, R.; Hrbáč, J.; Zbořil, R. The influence of complexing agent concentration on particle size in the process of SERS active silver colloid synthesis. *J. Mater. Chem.* **2005**, *15*, 1099–1105.

(5) Das, S. K.; Dickinson, C.; Lafir, F.; Brougham, D. F.; Marsili, E. Synthesis, characterization and catalytic activity of gold nanoparticles biosynthesized with *Rhizopus oryzae* protein extract. *Green Chem.* **2012**, *14*, 1322–1334.

(6) Li, S.; Shen, Y.; Xie, A.; Yu, X.; Qiu, L.; Zhang, L.; Zhang, Q. Green synthesis of silver nanoparticles using *Capsicum annuum* L. extract. *Green Chem.* **2007**, *9*, 852–858.

(7) Iravani, S. Green synthesis of metal nanoparticles using plants. *Green Chem.* **2011**, *13*, 2638–2650.

(8) Zhang, X.; Hu, J.; Jiang, H. Facile modification of a graphitic carbon nitride catalyst to improve its photoreactivity under visible light irradiation. *Chem. Eng. J.* **2014**, *256*, 230–237.

(9) Cui, Y.; Ding, Z.; Fu, X.; Wang, X. Construction of conjugated carbon nitride nanoarchitectures in solution at low temperatures for photoredox catalysis. *Angew. Chem., Int. Ed.* **2012**, *51*, 11814–11818.

(10) Cui, Y.; Huang, J.; Fu, X.; Wang, X. Metal-free photocatalytic degradation of 4-chlorophenol in water by mesoporous carbon nitride semiconductors. *Catal. Sci. Technol.* **2012**, *2*, 1396–1402.

(11) Li, X.-H.; Wang, X.; Antonietti, M. Mesoporous g-C_3N_4 nanorods as multifunctional supports of ultrafine metal nanoparticles:

DOI: 10.1021/sc500646a
ACS Sustainable Chem. Eng. 2015, 3, 269–276

hydrogen generation from water and reduction of nitrophenol with tandem catalysis in one step. *Chem. Sci.* **2012**, *3*, 2170−2174.
(12) Wang, X.; Maeda, K.; Chen, X.; Takanabe, K.; Domen, K.; Hou, Y.; Fu, X.; Antonietti, M. Polymer semiconductors for artificial photosynthesis: Hydrogen evolution by mesoporous graphitic carbon nitride with visible light. *J. Am. Chem. Soc.* **2009**, *131*, 1680−1681.
(13) Lyth, S. M.; Nabae, Y.; Moriya, S.; Kuroki, S.; Kakimoto, M.-a.; Ozaki, J.-i.; Miyata, S. Carbon nitride as a nonprecious catalyst for electrochemical oxygen reduction. *J. Phys. Chem. C* **2009**, *113*, 20148−20151.
(14) Zhang, X. S.; Hu, J. Y.; Jiang, H. Facile modification of a graphitic carbon nitride catalyst to improve its photoreactivity under visible light irradiation. *Chem. Eng. J.* **2014**, *256*, 230−237.
(15) Ge, L.; Han, C.; Liu, J.; Li, Y. Enhanced visible light photocatalytic activity of novel polymeric g-C_3N_4 loaded with Ag nanoparticles. *Appl. Catal., A* **2011**, *409*−*410*, 215−222.
(16) Bai, X.; Zong, R.; Li, C.; Liu, D.; Liu, Y.; Zhu, Y. Enhancement of visible photocatalytic activity via Ag@C_3N_4 core−shell plasmonic composite. *Appl. Catal., B* **2014**, *147*, 82−91.
(17) Ge, L.; Han, C.; Liu, J.; Li, Y. Enhanced visible light photocatalytic activity of novel polymeric g-C_3N_4 loaded with Ag nanoparticles. *Appl. Catal., A* **2011**, *409*, 215−222.
(18) Liang, W.; Church, T. L.; Harris, A. T. Biogenic synthesis of photocatalytically active Ag/TiO_2 and Au/TiO_2 composites. *Green Chem.* **2012**, *14*, 968−975.
(19) Subramanian, V.; Wolf, E. E.; Kamat, P. V. Catalysis with TiO_2/gold nanocomposites. Effect of metal particle size on the Fermi level equilibration. *J. Am. Chem. Soc.* **2004**, *126*, 4943−4950.
(20) Auffan, M.; Pedeutour, M.; Rose, J.; Masion, A.; Ziarelli, F.; Borschneck, D.; Chaneac, C.; Botta, C.; Chaurand, P.; Labille, J.; Bottero, J. Y. Structural degradation at the surface of a TiO_2-based nanomaterial used in cosmetics. *Environ. Sci. Technol.* **2010**, *44*, 2689−2694.
(21) Bone, A. J.; Colman, B. P.; Gondikas, A. P.; Newton, K. M.; Harrold, K. H.; Cory, R. M.; Unrine, J. M.; Klaine, S. J.; Matson, C. W.; Di Giulio, R. T. Biotic and abiotic interactions in aquatic microcosms determine fate and toxicity of Ag nanoparticles: part 2−toxicity and Ag speciation. *Environ. Sci. Technol.* **2012**, *46*, 6925−6933.
(22) Lan, J.; Zhou, X.; Liu, G.; Yu, J.; Zhang, J.; Zhi, L.; Nie, G. Enhancing photocatalytic activity of one-dimensional $KNbO_3$ nanowires by Au nanoparticles under ultraviolet and visible-light. *Nanoscale* **2011**, *3*, 5161−5167.
(23) Luan, J.; Li, M.; Ma, K.; Li, Y.; Zou, Z. Photocatalytic activity of novel Y_2InSbO_7 and Y_2GdSbO_7 nanocatalysts for degradation of environmental pollutant rhodamine B under visible light irradiation. *Chem. Eng. J.* **2011**, *167*, 162−171.
(24) Hong, J.; Xia, X.; Wang, Y.; Xu, R. Mesoporous carbon nitride with in situ sulfur doping for enhanced photocatalytic hydrogen evolution from water under visible light. *J. Mater. Chem.* **2012**, *22*, 15006−15012.
(25) Kuai, L.; Geng, B.; Chen, X.; Zhao, Y.; Luo, Y. Facile subsequently light-induced route to highly efficient and stable sunlight-driven Ag-AgBr plasmonic photocatalyst. *Langmuir* **2010**, *26*, 18723−18727.
(26) Liu, G.; Yan, X.; Chen, Z.; Wang, X.; Wang, L.; Lu, G. Q.; Cheng, H.-M. Synthesis of rutile−anatase core−shell structured TiO_2 for photocatalysis. *J. Mater. Chem.* **2009**, *19*, 6590−6596.
(27) Shih, Y.; Lin, C. Effect of particle size of titanium dioxide nanoparticle aggregates on the degradation of one azo dye. *Environ. Sci. Pollution Res.* **2012**, *19*, 1652−1658.
(28) Turner.; et al. Selective oxidation with dioxygen by gold nanoparticle catalysts derived from 55-atom clusters. *Nature* **2008**, *454*, 981−983.
(29) Mei, Y.; Sharma, G.; Lu, Y.; Ballauff, M. High catalytic activity of platinum nanoparticles immobilized on spherical polyelectrolyte brushes. *Langmuir* **2005**, *21*, 12229−12234.
(30) Zhao, J.; Wu, T.; Wu, K.; Oikawa, K.; Hidaka, H.; Serpone, N. Photoassisted degradation of dye pollutants. 3. Degradation of the cationic dye rhodamine B in aqueous anionic surfactant/TiO_2 dispersions under visible light irradiation: Evidence for the need of substrate adsorption on TiO_2 particles. *Environ. Sci. Technol.* **1998**, *32*, 2394−2400.
(31) Kapoor, S. Preparation, characterization, and surface modification of silver particles. *Langmuir* **1998**, *14*, 1021−1025.
(32) Vukovic, V. V.; Nedeljkovic, J. M. Surface modification of nanometer-scale silver particles by imidazole. *Langmuir* **1993**, *9*, 980−983.
(33) Awazu, K.; Fujimaki, M.; Rockstuhl, C.; Tominaga, J.; Murakami, H.; Ohki, Y.; Yoshida, N.; Watanabe, T. A plasmonic photocatalyst consisting of silver nanoparticles embedded in titanium dioxide. *J. Am. Chem. Soc.* **2008**, *130*, 1676−1680.
(34) Hu, C.; Peng, T.; Hu, X.; Nie, Y.; Zhou, X.; Qu, J.; He, H. Plasmon-induced photodegradation of toxic pollutants with Ag−AgI/Al_2O_3 under visible-light irradiation. *J. Am. Chem. Soc.* **2009**, *132*, 857−862.
(35) Wang, P.; Huang, B.; Qin, X.; Zhang, X.; Dai, Y.; Wei, J.; Whangbo, M. H. Ag@AgCl: A highly efficient and stable photocatalyst active under visible light. *Angew. Chem., Int. Ed.* **2008**, *47*, 7931−7933.
(36) Hu, C.; Hu, X.; Wang, L.; Qu, J.; Wang, A. Visible-light-induced photocatalytic degradation of azodyes in aqueous AgI/TiO_2 dispersion. *Environ. Sci. Technol.* **2006**, *40*, 7903−7907.
(37) Wang, Y.; Wang, X.; Antonietti, M. Polymeric graphitic carbon nitride as a heterogeneous organocatalyst: from photochemistry to multipurpose catalysis to sustainable chemistry. *Angew. Chem., Int. Ed.* **2012**, *51*, 68−89.

DOI: 10.1021/sc500646a
ACS Sustainable Chem. Eng. 2015, 3, 269−276